Probing the Stability of Ladder-Type Coilable Space Structures

Fabien Royer * and Sergio Pellegrino †
California Institute of Technology, Pasadena, CA, 91125

This paper analyzes the buckling and post-buckling behavior of ultralight ladder-type coilable structures, called strips, composed of thin-shell longerons connected by thin rods. Based on recent research on the stability of cylindrical and spherical shells, the stability of strip structures loaded by normal pressure is studied by applying controlled perturbations through localized probing. A plot of these disturbances for increasing pressure is the stability landscape for the structure, which gives insight into the structure's buckling, post-buckling, and sensitivity to disturbances. The probing technique is generalized to higher order bifurcations along the post-buckling path, and low-energy escape paths into buckling that cannot be predicted by a classical eigenvalue formulation are identified. It is shown that the stability landscape for a pressure-loaded strip is similar to the landscape for classical shells, such as the axially-loaded cylinder and the pressure-loaded sphere. Similarly to classical shells, the stability landscape for the strip shows that an early transition into buckling can be triggered by small disturbances however, while classical shell structures buckle catastrophically, strip structures feature a large stable post-buckling range.

Nomenclature

A	=	total area of strip
A_{BL}	=	area of longeron webs and battens
b	=	batten cross-section width
d	=	longeron cross-section web width
h	=	batten cross-section height
L	=	strip length
P	=	pressure applied on area A
P_{AB}	=	pressure applied on area A_{BL}
P_{cr}	=	non-linear buckling pressure

*Currently at MIT AeroAstro, 125 Massachusetts Ave, Cambridge, MA 02139. fabienr@mit.edu AIAA Member.
†Joyce and Kent Kresa Professor of Aerospace and Professor of Civil Engineering, Graduate Aerospace Laboratories, California Institute of Technology (GALCIT), 1200 E California Blvd. MC 105-05. sergiop@caltech.edu AIAA Fellow.
A preliminary version was presented as paper AIAA 2020-1437 at the AIAA Scitech 2020 Forum, Orlando, FL, 6-10 January 2020

P_{cr-lin} = linear buckling pressure

P_M = Minimum post-buckling pressure

P_{max} = Maximum post-buckling pressure

r = longeron cross-section radius

s = batten spacing

t = longeron flange thickness

W = strip width

Z = probe location along strip axis

θ = longeron cross-section opening angle

Terminology

Brief descriptions of the key terminology used in the paper are provided here.

- **Linear buckling eigenvalue/load**: buckling eigenvalue estimate obtained by solving the buckling eigenvalue problem for the undeformed structure.
- **Non-linear buckling eigenvalue/load**: buckling eigenvalue estimate obtained by iteratively solving the buckling eigenvalue problem as the structure is loaded. A first buckling eigenvalue prediction is performed without any pre-load. This first estimate gives the linear buckling eigenvalue. The structure is then pre-loaded under the linear buckling eigenvalue and a second buckling eigenvalue prediction is performed. This step is repeated until the pre-load converges to the buckling eigenvalue estimate, to give the non-linear buckling eigenvalue. The associated mode shape is denoted as the non-linear buckling mode.
- **Minimum post-buckling load**: load at which a specific post-buckling path restabilizes. This is the lowest load reached on the post-buckling path, unless no stable paths exist in the post-buckling regime. Note that the structure can reach lower load values if there exist bifurcations on the stable post-buckling path. In this case, one will associate one minimal post-buckling load with each bifurcation.
- **Maximum post-buckling load**: ultimate load that can be sustained by a structure before it loses its overall stiffness.

I. Introduction

Thin-shell structures have been used extensively for aerospace applications as they enable lightweight vehicles. Since the early 1920s, discrepancies between shell buckling experiments and theoretical buckling predictions based on linear bifurcation analysis based on perfect shell geometries were observed. The experimental buckling loads were lower than the analytical predictions and the discrepancy was later linked to the presence of initial imperfections in the shell geometry [1–3]. Considerable efforts were made to find safe lower bounds for the buckling load of these structures,

which led to the NASA space vehicle design criteria for the buckling of thin-walled circular cylinders (NASA SP-8007) [4].

Today, these empirical buckling criteria are still used but are seen as very conservative, and have some inherent limitations. To address these shortcomings, the NASA's Shell Buckling Knockdown Factor (SBKF) Project was established in 2007 to develop less-conservative, robust shell buckling design factors by testing shells with known imperfections, as well as non-uniformities in loading and boundary conditions [5]. The introduction of precisely engineered imperfections in spherical shells showed that buckling could be accurately predicted if the initial geometry is known accurately [6]. However, in many applications, measuring the shape of the structure before use can be both expensive and difficult. The traditional buckling and post-buckling prediction method uses a linear combination of the first buckling modes as imperfection [7, 8] and showed increased accuracy compared to the classical linear bifurcation approach. The importance of local deformations at the onset of buckling was linked to localization effects that cannot be described as a combination of eigenmodes [9].

In particular, post-buckling paths exhibiting localization are found in cylindrical and spherical shells. In most cases, these paths are broken away from the fundamental path but approach it asymptotically, and can be reached before the first eigenvalue is attained if a small amount of disturbing energy is input into the structure [10, 11]. For these early buckling routes, the structure exhibits a single dimple localized deformation and sits on a ridge of total potential energy separating the pre-buckling energy well and a lower energy, localized post-buckling well. This mode of deformation is thus called mountain pass point and it has been shown that the single dimple corresponds in fact to the cylindrical shell lowest mountain pass point [10], i.e. the post-buckling solution that can be reached with a minimal energy barrier. An experimental procedure to determine the fundamental path meta-stability was proposed in 2013 [12] and has been used experimentally [13]. Comparisons with earlier work showed that the onset of meta-stability often referred to as "shock sensitivity" [12] gives an accurate lower bound for experimental buckling loads [14, 15].

The objective of the present paper is to apply these recent breakthroughs in understanding cylindrical and spherical shell buckling to more complex thin shell structures made of composite materials. In particular, the present authors are currently investigating structural architectures for ultralight, coilable space structures for large, deployable, flat spacecraft for the Caltech Space Solar Power project (SSPP) [16]. In the deployed configuration, each spacecraft measures up to 60 m $\times$ 60 m in size and is composed of ultralight ladder-type coilable strips of equal width, arranged to form a square, and each strip supports photovoltaic and power transmission elements. This structure is described in a previous paper [17] and is shown in figure 1. Scaled laboratory prototypes of this structural concept have been built and tested [18, 19].

Ladder-type structures consist of two triangular rollable and collapsible (TRAC) [20] longerons, connected transversely by rods (battens), and will be referred to as a *strip* in this paper. In the proposed SSPP architecture, the strips are simply supported at the ends with boundary conditions that do not allow any tension to be applied. The battens are rectangular cross-section carbon fiber rods and the longerons are thin composite shells. The present study considers

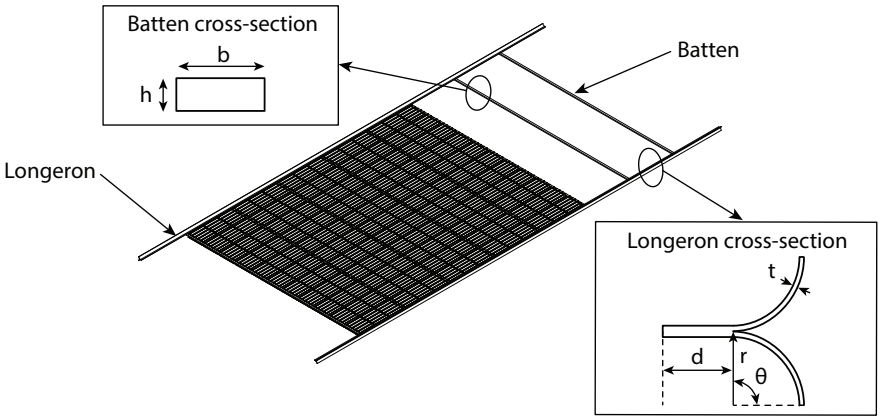

Fig. 1 Overview of ladder-type structure for SSPP.

a simplified version of the strips under development for SSPP, forming rectangles instead of trapezoids and with simpler boundary conditions.

In orbit, the main loading is solar pressure, modeled as a static pressure. This the main loading condition that will be considered in the present study. Dynamic load conditions can be modeled using an equivalent static pressure.

The purpose of the present study is to understand and quantify the buckling and post-buckling behavior of a strip, and explore the sensitivity of its transition to buckling, considering the effects of disturbances and imperfections. Recent work studied the longeron's deployed behavior and showed that localized buckles form under transverse bending, and that the post-buckling regime immediately after the first bifurcation restabilizes quickly. The studies focused on replicating experimental results using non-linear buckling an post-buckling simulations [21–24] and further work used non-linear buckling load computations coupled with modern machine learning techniques to design optimized longeron geometries [25].

The present paper takes a different approach. The stability of the pre-buckling (fundamental) path is assessed and insights into early transitions into the post-buckling regime are gained by using localized probing to apply a perturbation to the structure. The probing technique is then generalized to higher order bifurcations arising from the post-buckling path. Low energy escape paths into buckling that cannot be predicted by a classical eigenvalue problem are identified.

The paper is structured as follows. Section II highlights some experimental observations on the buckling of a cantilevered strip, to gain initial insights, and Section III reviews the concept of stability landscape for thin shell buckling, which is used in the rest of the paper. Section IV presents the numerical computation of stability landscapes for a specific strip structure with boundary conditions similar to those used for coilable strips, and Section V extends the use of these landscapes to the post-buckling regime. In Section VI the effect of the strip length on the stability landscape is investigated. Section VII generalizes the probing to the entire structure, unveiling the existence of low energy escape paths into buckling, similar to the low energy paths observed for the cylinder and the sphere. Finally, Section VIII presents a preliminary analysis of the effect of geometrical imperfections on the strip stability landscape.

II. Experimental observations on strip buckling

A 0.8 m long strip prototype with 3 battens spaced at 0.2 m was built and tested in the cantilever configuration shown in figure 2b. The longeron end cross-sections at one end of the structure were built into a stiff plate and the cross-sections at the other end were attached to a stiff composite rod. These boundary conditions did not allow the end cross sections to deform. Two load cells mounted on an acrylic beam were attached to a translation stage, and were placed in direct contact with the two longerons ends (using steel balls). When actuated, the linear stage displaced the two longeron ends and the reaction force at each end was measured. The end displacements of the longerons were also measured, using laser displacement gauges.

The results of this experiment are shown in figure 2a and the buckles that were observed are shown in figure 2b. It can be seen that longeron 2 is 10% softer than longeron 1, due to a slightly smaller cross-section introduced by the manufacturing process. The two longerons exhibit different buckling behaviors. A local buckle at the location of the first batten connection appears (buckle 1 in figure 2b) in longeron 2 for a tip deflection of 1.5 mm. As the tip deflection is increased, a gradual softening of longeron 2 is observed which physically corresponds to the growth of buckle 1. No other buckles appear in longeron 2. For longeron 1, the linear regime extends to a tip deflection of 2.5 mm, then the first buckle (buckle 2) appears close to the cantilever base. Unlike longeron 2, the behavior of longeron 1 after the appearance of buckle 2 is linear. A second buckle (buckle 3) appears 0.5 m away from the cantilever base, for a tip deflection of 8.5 mm. The postbuckling regime of longeron 1 after the formation of buckle 3 is also linear. Finally, unstable buckling of longeron 1 occurs for a tip deflection of 17.5 mm (buckle 4). At this point buckle 3 disappears. This ultimate buckling is of a different type and consists of a doubly-curved S-shaped flange deformation, which creates a localized region of very high curvature and leads to the formation of a crack at this location. Since the two longerons are connected at the tip by a carbon fiber tube, the drop in reaction force in longeron 1 is accompanied by a sudden increase of reaction force in longeron 2.

Based on this experiment, the following observations can be made regarding the behavior of the tested structure.

- Both longerons exhibited a long and stable post-buckling regime, until ultimate buckling occurred for a rather large tip deflection of 17.5 mm. For longeron 1, the ultimate buckling reaction force was 4.8 times larger than the first buckling reaction force, and 5 times larger for longeron 2. Each buckling event was quasi-static.
- The buckles forming in the longerons were very localized and consisted of a single wave. Therefore, local deformation played a key role in the buckling of the test structure, in analogy to the previously observed subcritical buckling behavior observed in spherical and cylindrical thin shells.
- Imperfections and deviations from the nominal geometry played a key role in the longeron behavior. Since more local variations in the shape of longeron 2 were observed, these imperfections were the likely origin of the gradual softening behavior observed in the experiment, as opposed to the sudden change of slope observed for longeron 1 (which has smaller shape deviations).

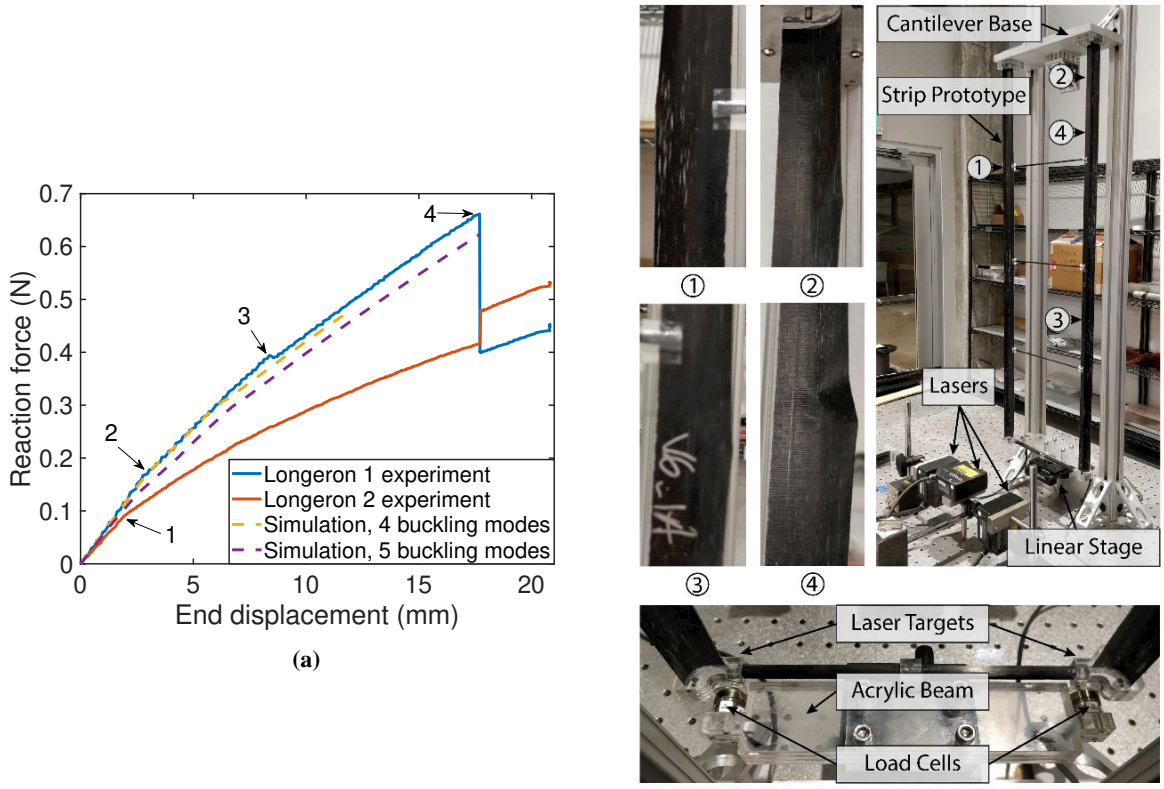

Fig. 2 (a)Reaction forces as a function of longeron tip displacement. (b) Experimental setup, local buckles and locations on longerons.

A finite element analysis was carried out to numerically reproduce some aspects of the experiment. A classical post-buckling approach was used, which consisted in seeding a linear combination of buckling modes into the longerons initial geometry to resolve the bifurcations and their post-buckling branches. Two attempts are shown in figure 2a, respectively using the first 4 and the first 5 non-linear buckling modes as imperfection. The total imperfection amplitude in the second attempt was about twice that used in the first attempt. The results shown refer to longeron 1. Qualitatively, the first attempt captured well the first buckling of longeron 1 but the the second post-buckling transition occurred much earlier than in the experiment. Convergence could no longer be achieved after a displacement of about 12 mm. Numerical convergence up to ultimate buckling was achieved but the imperfections needed to resolve all buckling events degrade the initial pre-buckling path, causing an early transition into the first post-buckling regime. These observations qualitatively highlight the difficulties encountered while trying to model a series of subsequent buckling events using seeded imperfections into the initial geometry [26].

This discussion indicates that it is important to quantify the post-buckling regime of strip structures, as significant load-carrying reserves may be available beyond the first buckling. This post-buckling response consists of multiple

localized buckles forming one after the other, and therefore, the probing methodology used to study localization in cylindrical and spherical shells seem to be particularly adapted to the study of the strip structure. This methodology is also helpful in overcoming the limitations of an imperfection-based simulation since no modification to the initial model geometry needs to be carried out.

III. General stability landscape approach to thin shell buckling

Recent work on thin cylindrical and spherical shell buckling has focused on the stability of the buckling phenomenon and its sensitivity to disturbances. Rather than seeing buckling purely as a bifurcation problem, these new contributions have studied in more detail the meta-stability of a structure's fundamental path and the early transition into adjacent post-buckling paths requiring small energy barriers to be overcome. A review of these recent advances has been presented by Groh et al [14].

Following these developments, the approach to shell buckling that is adopted in this paper uses the buckling stability landscape, a recently developed tool to study these phenomena. The notion of a stability landscape was introduced by Virot et al. [13] as a way to characterize the meta-stable nature of cylindrical thin-shell buckling. Virot et al. imposed a local radial displacement on a compressed cylinder, using a small ball probe (called a "poker" in [13]) which creates a localized single dimple. The stability landscape is the surface created when the probe force is plotted as a function of the probe displacement for various levels of the main loading parameter (axial compression or end-shortening of the cylinder). It provides a useful way to quantify the impact of probing on the buckling behavior and a general way to study buckling sensitivity of a structure to disturbances.

Even though the stability landscape was introduced for thin cylindrical shells, a similar landscape can be found for other types of shell buckling problems. A thin shell buckling stability landscape is sketched in figure 3a. For the specific scenario shown here, there exists a range of prescribed load for which stable equilibrium solutions exists. This is not always the case. The features of this landscape and their significance, described in [13], are briefly summarized next.

- **Point of spontaneous buckling**. This point corresponds to a zero probe displacement and the associated load is the non-linear buckling load. No disturbance is needed for the structure to transition into its post-buckling regime from this point.
- **Minimally buckled state**. The minimally buckled state corresponds to the load below which no buckles can form in the structure, whereas buckled states can exist above this load. This load corresponds to the load for which the probe force first falls to zero for a non-zero probe displacement. Below this load, the probe force does not drop to zero even for large probing displacements. Thus, the minimally buckled state represents the onset of metastability. This load can serve as an accurate bound for experimental buckling loads [14, 15].
- **Buckled equilibria solutions**. For loads above the minimally buckled state, there exist two states of equilibrium on the contour of probe force versus probe displacement where the probe force is zero for a non-zero probe

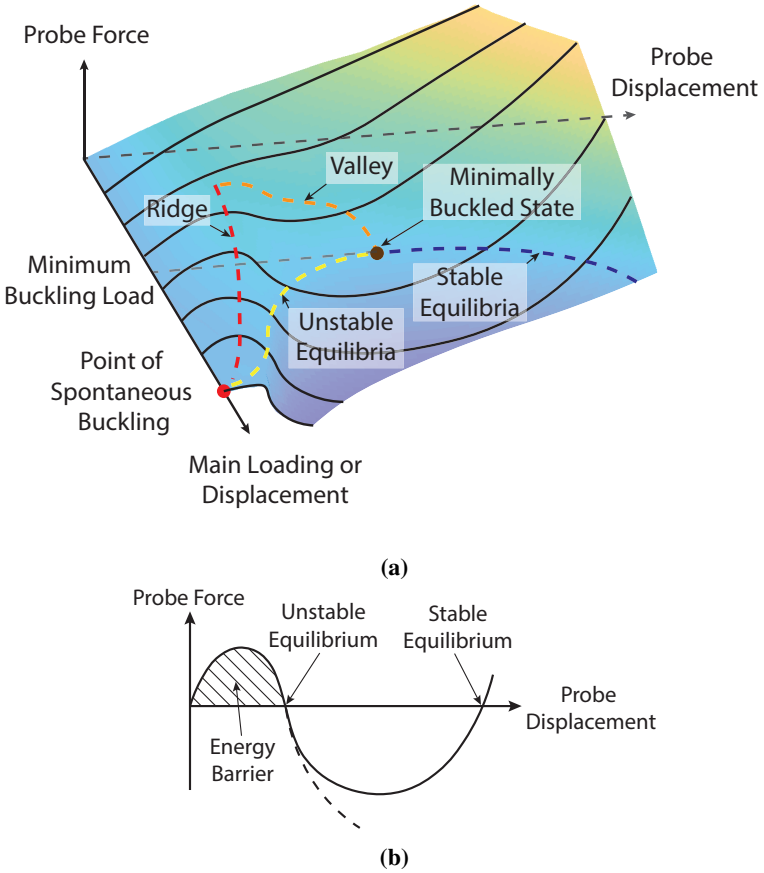

Fig. 3 (a) Schematic of thin-shell buckling stability landscape, reprinted with permission from [13]. Copyright 2017 by the American Physical Society. (b) Energy barrier between pre-buckled and post-buckled states, at a given level of loading.

displacement: an unstable state and a stable state. These two states are connected via the contour plotted in figure 3a. The two states coalesce at the load associated with the minimally buckled state. In a probing experiment where the probe is not glued to the structure, the structure will dynamically snap to the stable equilibrium state as soon as the probe attains the unstable equilibrium state. It is important to realize that the details of the stable buckled equilibrium state, and even its existence, depend on whether the overall loading applied to the structure is load-controlled or displacement-controlled (or some combination in between). For example, a spherical shell buckling under external pressure has a stable buckled state when loaded under volume-control but has no stable buckled state (other than complete collapse) under pressure-control. Note that the unstable equilibrium contour intersects the fundamental path at the point of spontaneous buckling in figure 3a. In some situations, offset post-buckling paths exist for which the unstable equilibrium contour never intersect the fundamental path. Such situations are discussed in Section VII.

- **Valley**. At loads below that associated with the minimally buckled state, a valley in the stability landscape is

associated with the local minima of the probe force. This contour of positive local minima terminates at the minimally buckled state.

- **Ridge**. The ridge is the locus of local maxima of the probe force. Each local maximum in the probe force is associated with an energy barrier between the stable unbuckled state and the unstable buckled state, as indicated in figure 3b. For any applied load, the energy barrier is the minimum energy that must be imparted to the structure by a disturbance to cause buckling. The energy barrier as a function of the applied load is directly related to the buckling sensitivity or "shock-sensitivity" [12] of the structure to disturbances. Note that the point of intersection between ridge and valley marks the appearance of a negative probing stiffness. At loads above this level, kinetic energy (snapping) would be released in a load-controlled probing experiment.

IV. Computation of strip stability landscape

A. Finite element model

A finite element model (FEM) of a strip, composed of two longerons of length L in the range 1.8 m to 4.2 m was developed. The geometry of the structure is described in figure 1. The cross-section has opening angle $\theta = 100$ deg, radius $r = 12.2$ mm, thickness $t = 98$ μm and web length $d = 8$ mm. The two longerons are connected by regularly spaced transverse rods, called battens, at spacing $s = 0.3$ m. The batten length is approximately equal to the width of the strip, $W = 0.2$ m, and its rectangular cross-section has width $b = 3$ mm and height $h = 0.6$ mm. The longeron flanges are made of a [±45 GFPW / 0 CF /±45 GFPW] laminate, known as FlexLam [27], where GFPW refers to glass fiber plain weave and CF refers to unidirectional carbon fiber. The two flanges are connected with a ply of glass fiber plain weave at the web.

The FEM was built using the Abaqus 2019 commercial software. The longerons were modeled with 4 node reduced integration shell elements (S4R) and the battens with linear 3D beam elements (B31).

B. Finite element analysis

The strip structure was held in a simply-supported condition, as shown in figure 4. The outer web edge (highlighted in orange) on one of the longeron cross-sections was prevented from translating in any direction while the web edges of all other end cross-sections were constrained in a way that allows the projections of the strip length and width onto the (xz) plane to vary. Details on these boundary conditions are provided in figure 4. Note that these boundary conditions are different from the cantilever experiment presented in Section II and, while the two problems bear some important similarities, they cannot be directly compared.

A uniform pressure was applied on the longeron webs and on the battens top faces. The total area loaded by pressure in the numerical model is A_{BL} (where BL denotes battens and longerons) and the associated buckling pressure is called P_{cr-AB} (were AB denotes Abaqus). However, in an actual structure a thin membrane would be attached to the edges of

the longerons and hence the loading (solar pressure) would act on the entire area $A = L \times W$ spanned by the structure.

In order to emphasize the practical significance of the present study, all results are presented in terms of P, although P_{AB} is actually used in the analysis. The two pressure values are related by $P \times A = P_{AB} \times A_{BL}$.

For each value of P, the top edge of the longerons was probed by applying a transverse nodal displacement U_{xp} at $Z = Z_p$, and the probe reaction force was extracted. The two independent control parameters to construct the stability landscape are therefore the pressure and the probe displacement. Probing a spatially extended region, using pressure for instance, has not been considered in the present study. From a practical standpoint, probing at a point can easily be implemented by using a small wedge that contacts the top edge of the longeron, with the axis of the wedge chosen perpendicular to the longeron's edge.

All the analyses were performed using the Abaqus implicit solver, in a static mode. The pressure was applied as a load, whereas the probes were modeled as displacement boundary conditions. An automated step size was used for both pressure loading and probing, and no numerical damping was introduced.

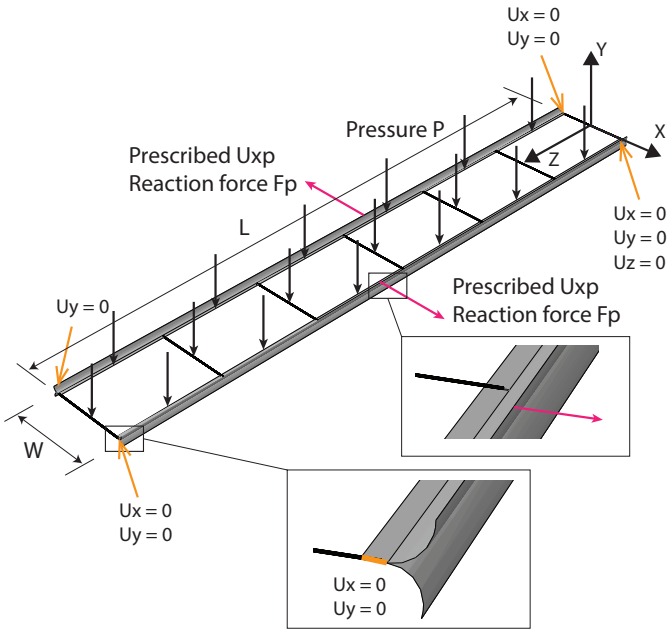

Fig. 4 Schematic of FEM for strip of coilable space structure, loaded by pressure.

The last important consideration is the choice of the probe locations. In a classical buckling and post-buckling analysis, one would compute non-linear buckling eigenmodes and seed a linear combination of these modes into the structure's initial geometry [7]. The use of an arclength solver coupled with the imperfect geometry enables tracing the first bifurcation branch. The early transition into such a branch, governed by the structure's non-linear eigenmodes, was studied first. Therefore, the probing location was first chosen as the location at which the peak deformation for the first eigenmodes is reached.

The first non-linear eigenmodes were obtained using the following iterative scheme. First, a buckling mode prediction

was performed for the undeformed structure to obtain the linear buckling load P_{cr-lin}. Next, a pressure of $0.5P_{cr-lin}$ was applied on the strip. A buckling prediction was then performed on the prestressed strip and a new value of the critical buckling load was then computed. This process was repeated until the pressure applied before the buckling prediction step had converged, thus obtaining the non-linear buckling pressure. The analysis yields two eigenvalues, corresponding to four eigenmodes. The first eigenvalue corresponds to a pair of two different buckling modes featuring local buckles on longeron 1 and longeron 2, localized on either side of the central batten. These modes are shown in figure 5a. They are labelled mode 1 longeron 1 and mode 1 longeron 2, and they correspond to the same value of the critical pressure. Similarly, the second eigenvalue corresponds to a pair of modes. The highly localized nature of these eigenmodes could be explained by the pressure loading causing a non-uniform bending moment along the strip length, which reaches a maximum magnitude at the center of the structure. In order to study early post-buckling branches associated with such modes, the probe location was chosen as the location of maximum displacement for these modes.

Two probing schemes were considered in the present study, as shown in figure 5b. The antisymmetric probing scheme uses one probe per longeron. The location of this probe matches the peak displacement of the first buckling mode for each longeron. The symmetric probing scheme uses two probes on each longeron and the probe displacements are all equal. The probe locations are given by the location of peak displacement for the first two buckling modes. In both probing schemes, the probes are displaced in the x-direction, in an outward sense. Note that the computed modes are combinations of inward and outward flange deflections. By conducting a conventional numerical post-buckling analysis based on a linear combination of these modes seeded in the perfect geometry, it was observed that the deformed shape obtained from the first bifurcation branch featured only outward buckles. This motivated the choice of the outward probing scheme, but it should be noted that restricting the chosen probing scheme to these modes, has the effect of restricting the scope of the meta-stability study. There is no guarantee that this approach yields the lowest transition into buckling, and a more complete set of probing schemes would be needed to have a full picture of the complex buckling behavior of such structure. A less restrictive approach, that does not use the eigenmodes to choose the probing location is presented in Section VII.

An even more general approach would use a single probe for the entire structure. In most cases, complete buckling modes feature several local buckles, which in practice appear one after the other, in a series of destabilizations and restabilizations called a snaking sequence [14]. We have limited the scope of the present study to the simultaneous formation of the buckles constituting an eigenmode, and the use of a single probe will be investigated in future work. While being less general, the current probing scheme has the advantage of limiting the scope for global instabilities, as discussed in Section IV.D.

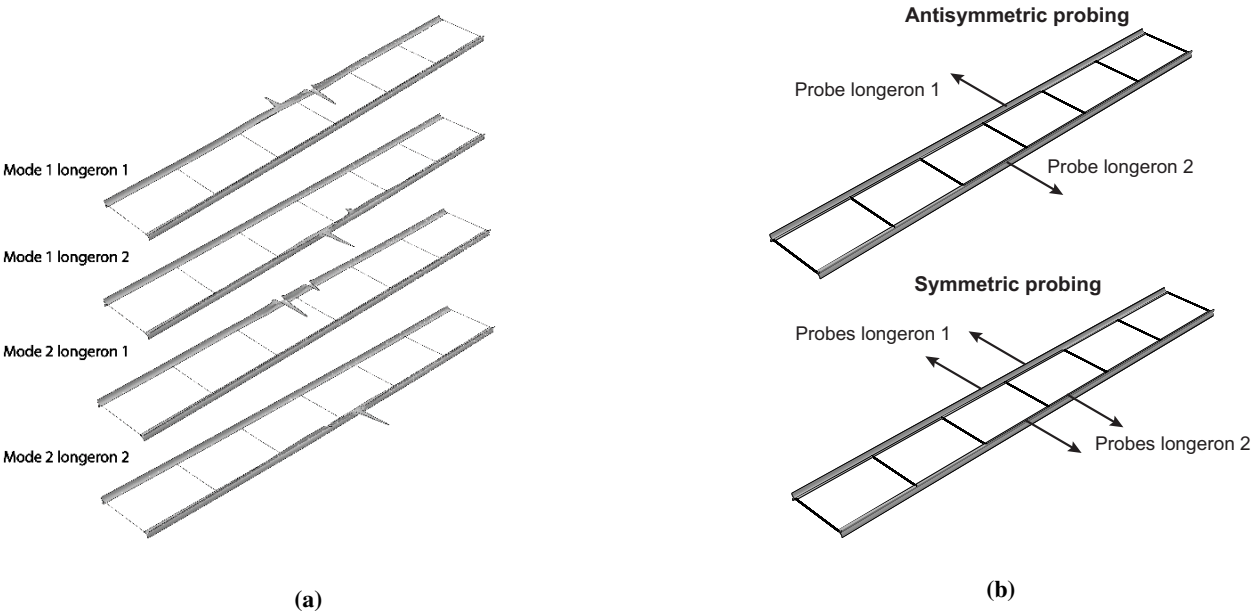

Fig. 5 (a) First 4 non-linear buckling modes for L = 1.8 m. (b) Symmetric and antisymmetric probing schemes derived from these modes.

C. Stability landscape

Plotting the reaction force as a function of the probe displacement for several values of the applied pressure load generates the stability landscape for the strip. This section focuses on a 3 m long strip for which the stability landscape for antisymmetric probing is shown in figure 6, the landscape for symmetric probing is similar. All the features described in the Introduction and Section III can be seen here. The obtained minimum post-buckling load for this specific strip length is $P_M = 0.86$ Pa. The ridge, fundamental path and unstable equilibrium contour intersect at the non-linear buckling load $P_{cr} = 1.45$ Pa.

It is interesting to note that the values of critical probe displacement obtained in the present study are similar to the values obtained for industrial cylindrical cans [13]. However, in the present study the open cross-section of the longerons lowers the ridge probe force magnitude about two orders of magnitude beneath the cylindrical cans [13], where ridge forces of about 1 N were found just above the minimum post-buckling load.

It is important to mention that in the case of other boundary conditions, the specific values of buckling loads and the locations at which local buckles appear will likely change. However, the stability landscape is expected to remain qualitatively the same, and the probing methodology can be applied again to obtain updated values of the buckling loads.

Finally, it has to be noted that the shape and features of the stability landscape would change if the probe location is offset from the location of the eigenmode peak deformation, even by a small amount. It has been observed experimentally that the stability landscape forms a fold, corresponding physically to the propagation of a buckle. This phenomenon and its implications will be fully described in a future publication.

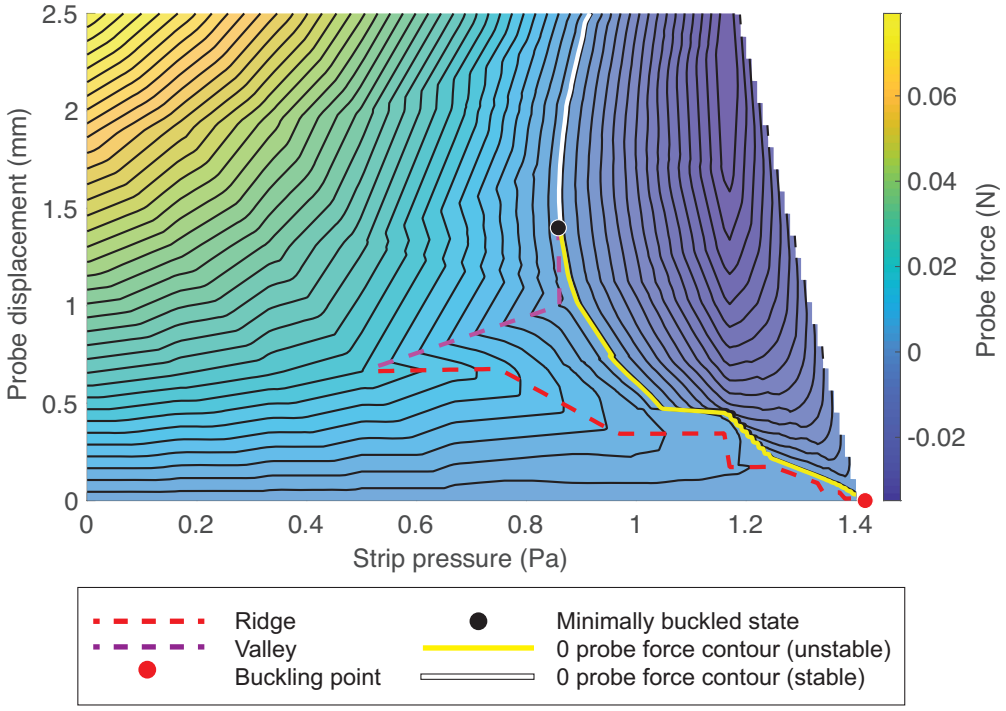

Fig. 6 Stability landscape for 3 m long strip structure, for antisymmetric probing.

D. Probing instabilities

The previous subsection has presented the stability landscape for antisymmetric probing of a strip with $L = 3$ m. In the nominal probing scheme, the structure remains straight and planar and the two probe forces are equal, such that there is no net force resultant on the structure (although there is a moment resultant for the antisymmetric probing scheme).

Bifurcations were encountered on the main probing path, in the immediate vicinity of the unstable equilibrium point (first appearance of 0 probe force). They are reported in figure 7 with their corresponding mode shapes, for an applied pressure $P = 1.17$ Pa. Two types of instabilities can be seen. The first one is linked to the first and second eigenvalues, and involves an interaction between local flange instabilities at the probe location, and in-plane bending of the entire structure. This type of interaction arises from the low in-plane bending of the strip structure. The second type of instabilities are purely local and are triggered by the third and fourth eigenvalues. In the case of the first and third eigenmode, a local symmetry breaking bifurcation occurs locally as the single wave dimple at the probe location transforms into an antisymmetric mode shape. This type of bifurcation has been observed before in other structures, such as an elastic arch under normal concentrated force. A classification of bifurcations and obstacles to a probing sequence has been provided by Thompson, Hutchinson and Sieber [28].

The cluster of eigenvalues near an unstable equilibrium solution gives rise to multiple probing paths. Two of these paths are highlighted in figure 8a. The deformed shapes following the dashed path are shown in figure 8b, for 4 different

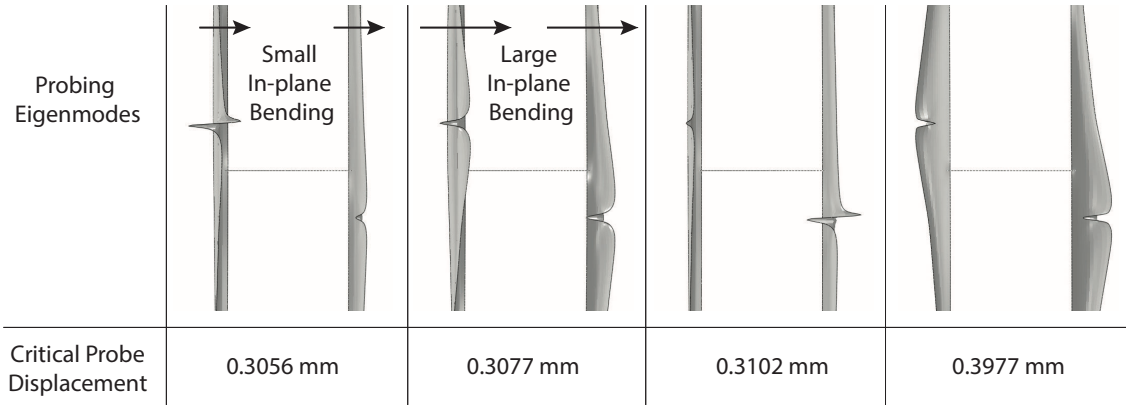

Fig. 7 Eigenvalues encountered during a probing sequence at P = 1.17 Pa.

probe displacements. One can observe that the behaviors of longeron 1 and 2 are identical until bifurcations are reached. In this initial probing regime, the buckle amplitude of both longerons grows and the probe force increases and then decreases towards the unstable equilibrium solution. Past the bifurcation, the behavior of longerons 1 and 2 are different. The structure starts bending in plane, as previously described, which results in an increase in the buckle amplitude for longeron 1 while longeron 2 deforms globally in bending. The paths shown by solid lines in the figure are essentially delayed version of the dashed paths, for which bifurcations occur in the range of negative probe forces. Once the bifurcation has been passed, the deformed shapes obtained for the solid line paths are similar to the ones for the dashed paths. These two sets of paths illustrate the local/global interaction that can disturb a probing sequence, but many other paths exist.

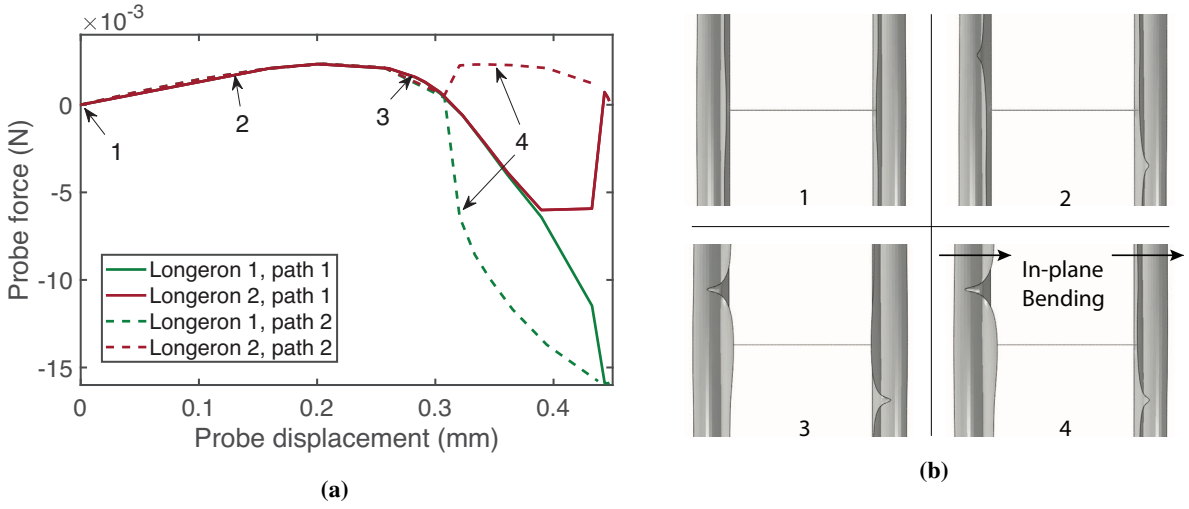

Fig. 8 (a) Two sets of probing paths for longeron 1 and 2 after encountering a bifurcations, for $P = 1.17$ Pa. (b) Deformed shapes at various points of the probing paths shown in (a).

These instabilities can be seen as limitations to the probing analysis, but in fact they highlight a powerful approach to selecting appropriate sets of constraints and boundary conditions for a given structure. In other words, these instabilities can be avoided by the judicious implementation of additional boundary conditions.

V. Generalization of stability landscape to post-buckling regime

A. Iterative computation of stability landscapes

The focus of this section is the ultimate pressure that can be carried by the strip structure which requires a study of the post-buckling response of the structure using stability landscapes. Knowledge of the structure's post-buckling behavior is the key to understanding whether buckling is benign or catastrophic.

Consider the stability landscape shown in figure 6. The unstable equilibrium solutions, defined by the yellow contour, determine the critical probe displacements needed to trigger local buckling. Past this critical displacement, the probe can be released and the structure will naturally snap into the stable equilibrium solutions, defined by the white contour. Once the stable equilibrium contour has been reached, the structure has transitioned into its post-buckling path. This transition can be implemented easily in the finite element analysis. Note that it differs from the classical approach, which consists in seeding imperfections in the structure's undeformed geometry, and using an arc-length solver to force the bifurcation into a specific branch. While the classical methodology is useful to obtain a rough idea of the structure's post-buckling behavior, it can be quite difficult to implement, as shown in Section II, because one does not have control over when the imperfect structure will bifurcate, and the post-buckling path is approximate since the structure's geometry has been changed. For imperfection sensitive structures (which include thin shell structures), these two effects are particularly pronounced and it becomes difficult to resolve higher-order bifurcation paths (i.e., bifurcations from the primary post-buckling branch) since the imperfections needed to resolve the higher-order bifurcations can modify the structure's behavior for earlier bifurcations. Path following methods [29] are extremely powerful in this respect, as they allow the exact post-buckling path for a structure to be traced. However these methods are available only in research finite element codes. An advantage of using the probing method adopted here is that it gives insights into the stability of the fundamental and post-buckling paths and their resilience to disturbances, while allowing resolution of the strip behavior after multiple bifurcations, and thus up to the ultimate failure pressure. It can also be implemented in experiments, which is of course a major advantage.

Once the structure starts following its first post-buckling path, its behavior can be be computed uniquely until a new bifurcation is encountered. At this point, a non-linear eigenvalue computation can be performed and the probing process can be repeated using the maximum amplitude location of these new eigenmodes to determine the new probing location. Note that once the $n-1$ buckle is fully formed, there is no more need to continue probing at its location and the $n-1$ probe can be released when the n probe is activated. This iterative process is repeated until the maximum pressure is

found.

This process is illustrated in figure 9, corresponding to the antisymmetric probing of figure 11a. A specific post-buckling path is shown but there exist infinite possible paths. Each path is associated with a specific level of disturbance and the associated energy barriers are reported in figure 9b. However, while the pressure at which probing is started sets the point at which the transition into buckling occurs, it does not affect the behavior of the structure after it reaches the stable equilibrium path. Therefore, for a specific probing scheme, the maximum pressure will be independent of the path chosen. Also, once a buckle is fully formed and the probe is released, the peak displacement of the buckle can still be tracked.

The peak displacements of the three buckles are shown by black curves in figure 9a, and the deformed shapes at points I, II, and III are shown in figure 10. Note that buckle 1 yields the largest deformation. Also note that global failure of the strip occurs when buckle 1 reaches a maximum value of outward displacement, at P_{max}. At this point, a localized fold forms at the center of the structure while the amplitudes of buckle 2 and 3 decrease, and the strip starts folding.

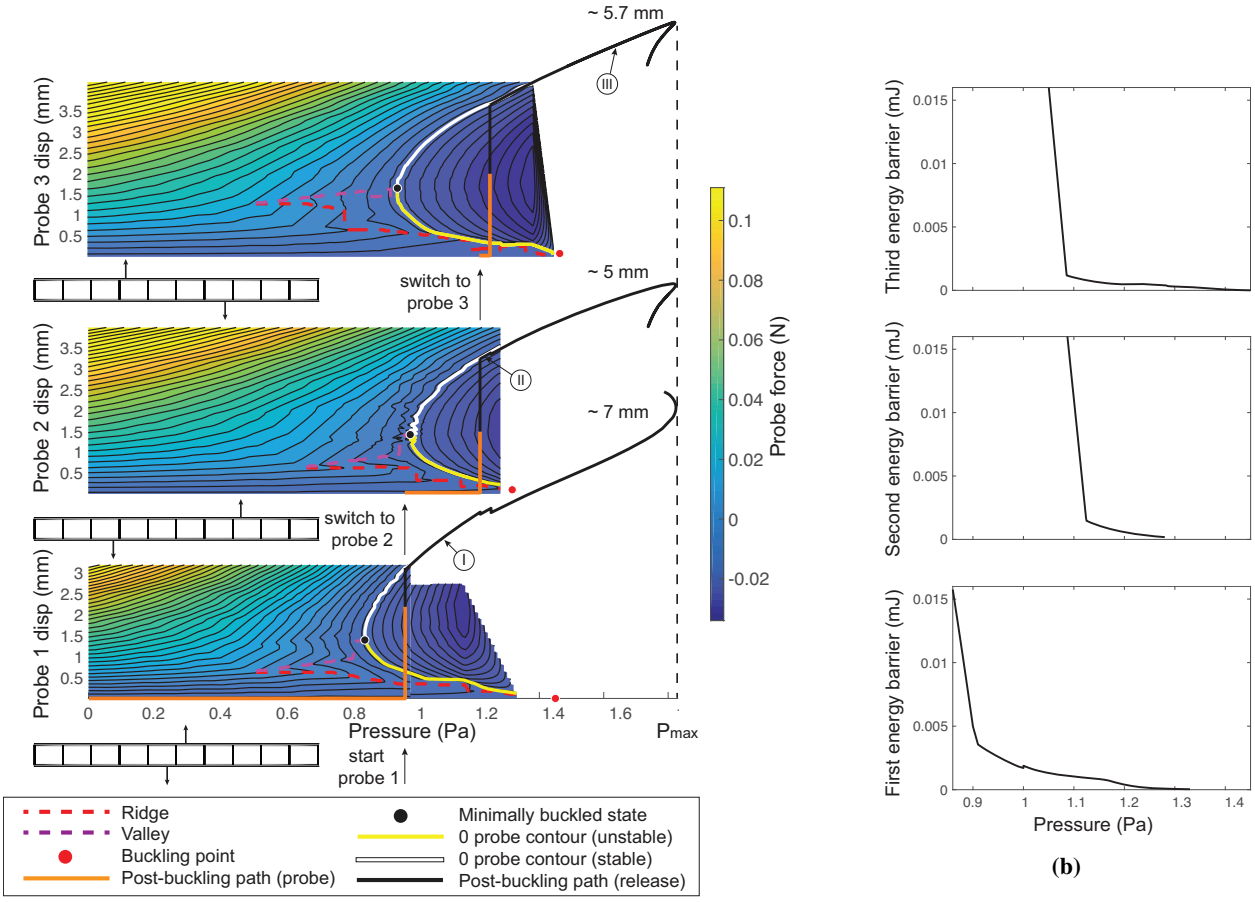

(a) (b)

Fig. 9 (a) Stability landscapes for the three sequential sets of probes. Labels I, II and III refer to the deformed shapes in figure 10. (b) Energy barriers for the 3 buckling transitions.

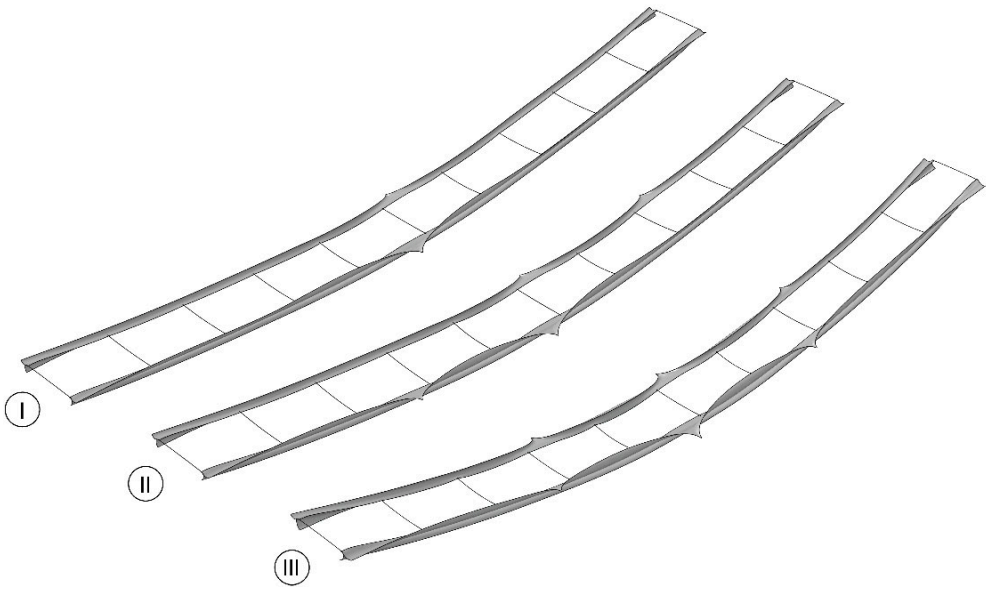

Fig. 10 Deformed shapes corresponding to points I, II and III of figure 9a. The displacements have been magnified by a factor of 5.

B. Post-buckling response for symmetric and anti-symmetric probing

The method described in the previous subsection was used to trace the structure's post-buckling response for symmetric and anti-symmetric probing. The antisymmetric probing starts as shown in figure 5b. The subsequent probes 2 and 3 are determined using the iterative method described earlier, by considering only the first eigenmode for each longeron. Similarly, the symmetric probing starts as shown in figure 5b and uses the first two eigenmodes to choose the probe locations, which results in using 4 probes at a time. These two probing schemes are shown in figure 11a.

The probing approach allows one to trace the full post-buckling response shown in figure 11b. The x-axis corresponds to the displacement extracted in the middle of the longeron (1.5 m from the end), at the cross-section centroid. The previously described failure of the structure appears as a horizontal tangent in this plot, which highlights the loss of stiffness at the maximum value of pressure. The deformed shapes, just before failure and for both types of probing, are shown in figure 12. Note that the antisymmetric probing scheme yields a softer post-buckling regime and a lower value of the maximum pressure. Thus, the antisymmetric probing scheme is the one to be considered when determining safe bounds on the structure's operational range.

In addition to the probing method, an attempt was made to compute the full antisymmetric post-buckling response using the "traditional" method, which consists in seeding the buckling modes shapes into the initial geometry. The result is shown by a black dashed line in figure 11b, for a total imperfection amplitude of 2% of the shell thickness. The probing and "traditional" techniques give essentially the same result for the first post-buckling branch. However, this simulation was not successful in going past the first post-buckling regime. Due to the structure's high imperfection

sensitivity, seeding the second buckling modes in the initial geometry (even for an imperfection amplitude of less than 0.5% of the shell thickness) degrades the pre-buckling response and first bifurcation can no longer be resolved. Finally, the numerical probing technique presented in this paper allows the structure to transition from its fundamental path directly to the stable post-buckling branch while the applied pressure is kept constant. Such a scheme, while numerically efficient, does not detect any potential bifurcations arising from the unstable post-buckling branch, as highlighted by Pirrera et al [30]. Such bifurcations could give rise to different stable post-buckling branches.

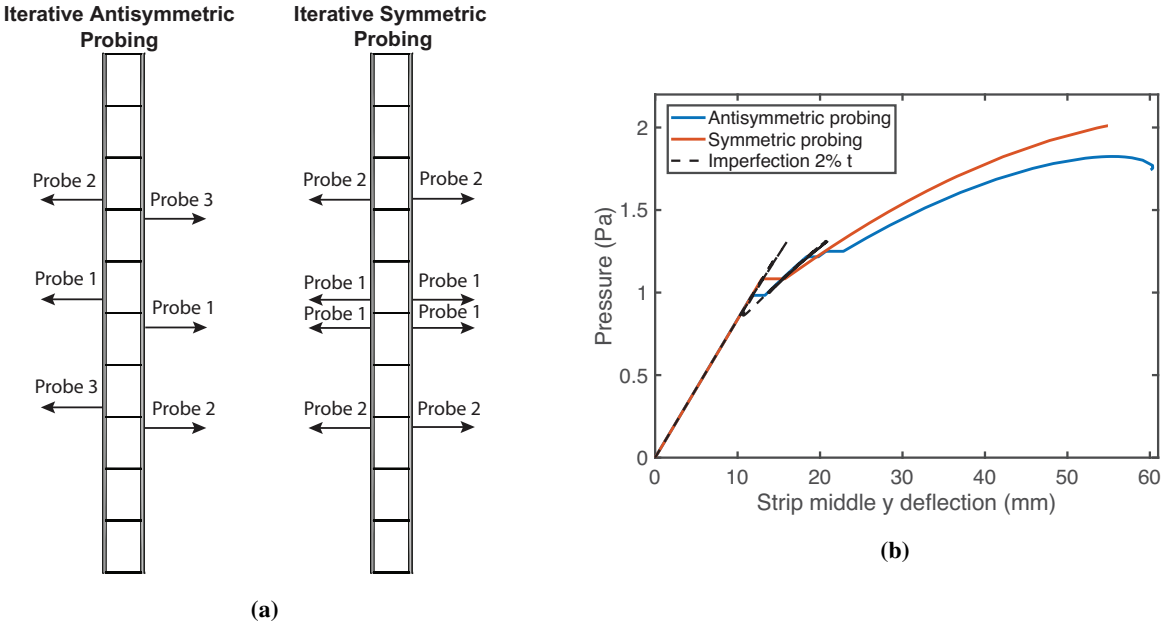

(a) (b)

Fig. 11 (a) Probing schemes for higher-order stability landscapes. (b) Full post-buckling response for the symmetric and antisymmetric probing scheme.

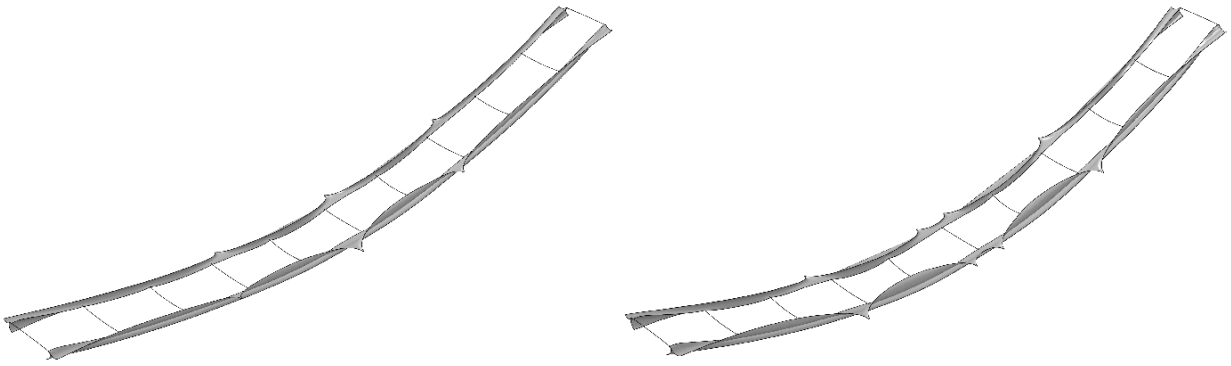

(a) (b)

Fig. 12 Deformed shape for (a) antisymmetric and (b) symmetric probing. The displacements have been magnified by a factor of 5.

To overcome this limitation, two approaches are taken. The first one consists in checking the eigenvalues of the tangent stiffness matrix, as the structure is probed. Any intersection with a new stable post-buckling branch will be

detected in this way, and the probing scheme can then be changed following the eigenmodes of this new bifurcation, before reaching the stable equilibrium contour of the previously determined bifurcation branching from the fundamental path. However, this approach is unable to detect unstable paths that do not restabilize since they do not intersect the probing path. The second approach consists in releasing the probe right before reaching the unstable equilibrium contour. The full unstable and stable branch can then be resolved using an arclength solver and one can directly check for negative eigenvalues on the unstable post-buckling branch. This second technique has been used successfully for different types of structure. For the ladder-type coilable structure no negative eigenvalues were detected while probing, and the preliminary experiment discussed in Section II suggests that there are no fully unstable paths leading to early failure before the ultimate pressure is reached.

VI. Effects of strip length on buckling energy barrier and characteristic loads

The analysis described in Section IV-B was repeated for lengths of 1.8 m, 4.2 m, 5.4 m and 6.6 m. The first quantity that has a direct impact on the early buckling of the structure is the minimum post-buckling pressure which was computed for all of the considered strip lengths. The evolution of the linear and non-linear buckling pressures was also tracked. Finally, by computing the full post-buckling response of the structure, the maximum post-buckling load was determined.

The evolution of these four quantities as a function of L is shown in figure 13a. This figure shows that the linear and non-linear buckling pressures decrease as the strip length increases, with the linear buckling pressure (eigenvalue problem for the undeformed structure) slowly converging to the non-linear buckling pressure and the eigenmodes also become very similar. While the first non-linear eigenmodes localize on a side of the central batten, the linear eigenmodes are symmetric with respect to the central batten. As the length of the strip increases, the non-linear buckling modes become less localized and more symmetric with respect to the central batten, as shown in figure 14.

Comparing the non-linear eigenmodes in figure 14 with the post-buckling deformed shapes in figure 10 it can be noted that the non-linear eigenmode has multiple peaks of decreasing amplitude, whereas the deformed shape I in figure 10 features only a single buckle. This type of localization has been studied for various problems, including elastic beams on an elastic foundation [31] and spherical shells [32].

A second observation is that the ultimate buckling pressure decreases as L increases. When looking at the formation of local buckles in the post-buckling regime, it is observed that the longer the strip, the more buckles are formed before reaching the ultimate buckling load. Since the formation of a buckle in the structure is associated with a decrease in stiffness, the structure will reach a zero value of stiffness earlier if more buckles can form, since the minimum buckling pressure for higher-order buckles does not increase significantly (see Section V.B). The ultimate buckling load is about 1.39% greater than the non-linear buckling load for L = 1.8 m and only 1.26% greater for L = 4.2 m.

As L increases, a similar decrease in the minimum post-buckling pressure is observed. Notice that the ultimate

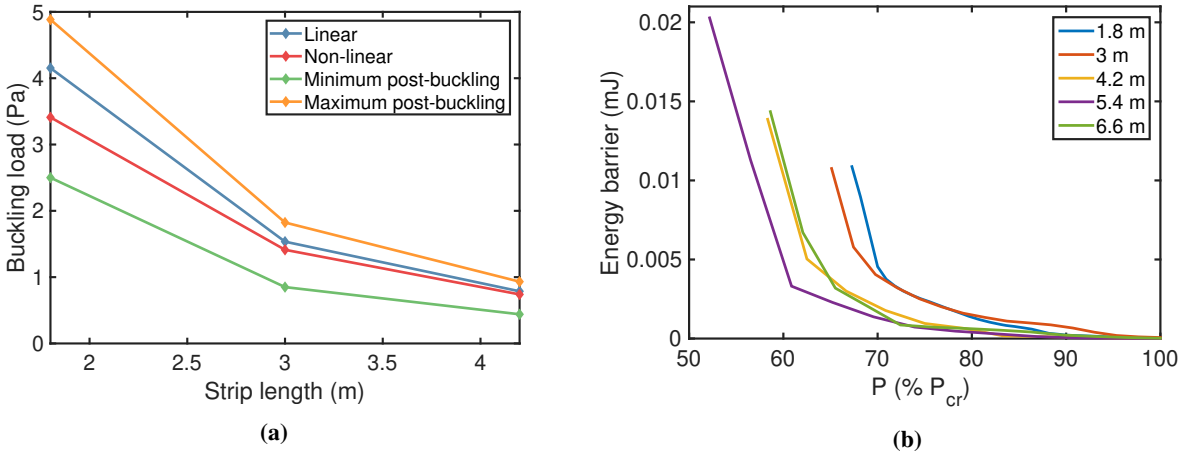

Fig. 13 Evolution of (a) critical loads and (b) energy barrier as a function of L.

buckling load converges faster to the non-linear buckling load than the minimum post-buckling pressure.

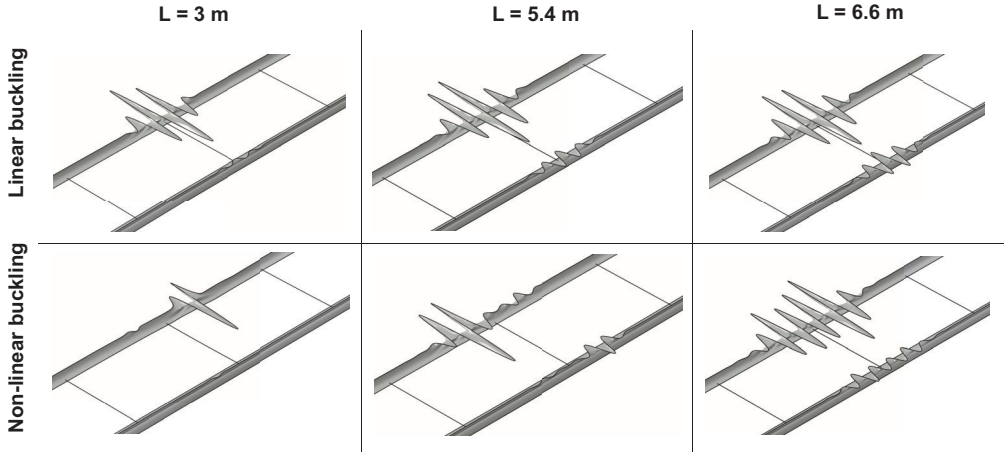

Fig. 14 Comparison between linear and non-linear buckling mode shapes for 3 different lengths.

The energy barrier against the buckling transition into the antisymmetric first mode at $P < P_{cr}$ has been plotted in figure 13b for the various strip lengths considered. The shape of the barrier is consistent across the different lengths and follows qualitatively the same trend as the minimum post-buckling pressure. A rather surprising effect is that, whereas the minimum post-buckling pressure and energy barrier decrease when L is increased up to $L = 5.4$ mm, the opposite trend is observed when L is increased further to 6.6 m. This result indicates that the minimum post-buckling pressure and the energy barrier are not monotonic with respect to the strip length.

The results obtained in this section can be linked to the spacecraft design application described in the Introduction. In figure 15, the linear buckling pressure for a range of strip lengths and widths has been compared to the value of 9×10^{-6} Pa, which corresponds to the solar radiation pressure on a spacecraft orbiting the earth (denoted as 1 astronomical unit, or 1 au). This loading has been chosen as a mean of comparison since it does not depend on a specific

mission scenario. However, note that inertial forces caused by attitude maneuvers may in practice be more critical than solar pressure, and these loading contributions will need to be assessed and compared for each specific mission scenario. For narrow strips ($W < 0.6$ m), buckling takes the form of a localized longeron buckling, as previously described. In wider strips ($W > 0.6$ m) the battens are longer and tend to buckle before the longerons, which gives rise to a plateau in the linear buckling pressure for shorter strips. The evolution of the linear buckling pressure for longer strips is consistent over the range of strip lengths. For $W = 1$ m and $L = 12$ m, the linear buckling pressure is 2215 times greater than the solar pressure, for $L = 30$ m it is 434 times greater, and for $L = 60$ m it is 333 times greater. These results indicate that the risk of buckling under solar pressure is very small for all lengths considered. However, for these longer strips, the linear buckling mode takes the form of a global periodic twisting of the strip along its axis and the non-linear localization effects may possibly yield significantly lower non-linear buckling loads.

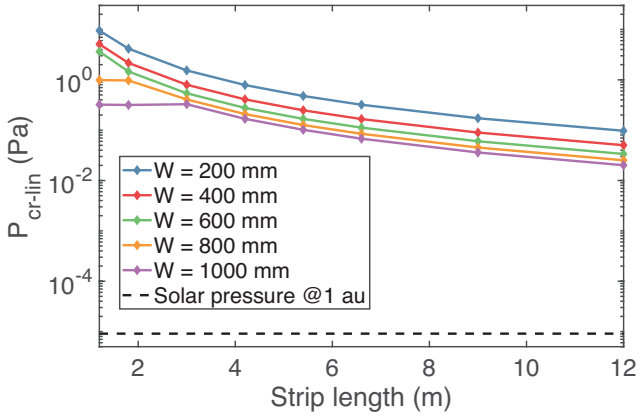

Fig. 15 Linear buckling pressure as a function of strip length and strip width.

VII. Low energy escape paths

The previous part of this study has analyzed early transitions into post-buckling, corresponding to the first non-linear buckling modes. However, while these modes give rise to a meta-stable fundamental path above the minimum post-buckling pressure, there may exist additional meta-stable paths in the immediate vicinity of the fundamental path that are also associated with a very low energy barrier, and which would yield an earlier transition into the post-buckling regime. Such *broken away* paths were recently studied for the case of the cylindrical shell under axial compression and for the spherical shell under pressure [33–35]. In the case of the cylinder the corresponding mode shapes take the form of a localized dimple.

Unstable broken away paths run close to the fundamental path without ever intersecting it, and therefore cannot be predicted by a bifurcation analysis [36]. The points forming such paths are referred to as *mountain pass points, because they correspond to the lowest point on a ridge in the total potential energy map for a fixed value of loading [14].* This

ridge separates the fundamental well from a lower potential well corresponding to a localized buckling mode, and the mountain pass points correspond to an unstable equilibrium contour in the probe force stability landscape. The mountain pass point requiring the least amount of energy to be reached is called the lowest mountain pass point and for the cylinder it has been shown that the single dimple solution is indeed the lowest mountain pass point [10].

In order to search for broken away paths and mountain pass points for the strip structure, the finite element analysis described in Section II.B was extended to multiple probe locations. For $L = 3$ m, 39 different probe locations (one probe location every 75 mm) were defined along the top edge of each longeron, with the Z-coordinate defining their position and a second probe was applied to the second longeron, in the same outward anti-symmetric arrangement described in Section IV.B. The probe force for each probe location and for different values of the applied pressure was obtained from the analysis and the energy barrier was computed as described in Section III, Figure 16a is a plot of the energy barrier as a function of the probe location Z and the applied pressure.

Focusing first on pressures close to the non-linear buckling pressure ($P = 1.1 - 1.3$ Pa) three plots of the energy barriers for varying Z are shown in figure 16b. The local minima, labeled A1, A2, occur for $Z = 1,423,\ \ 1,579$ mm, corresponding to the first buckling modes. For $P = 1.33$ Pa, there exist two more local minima further away from the center of the strip and labeled B1, B2, at $Z = 1,120$ and $1,880$ mm. These local minima are relatively high compared to the buckling mode minima for $P = 1.167$ Pa, but they quickly drop to comparable values for $P = 1.33$ Pa. This result indicates that buckling could occur also at these locations for a small disturbance, instead of the main disturbances near the center of the strip. However, note that for this range of pressures, the disturbances corresponding to the buckling modes still correspond the lowest energy barrier.

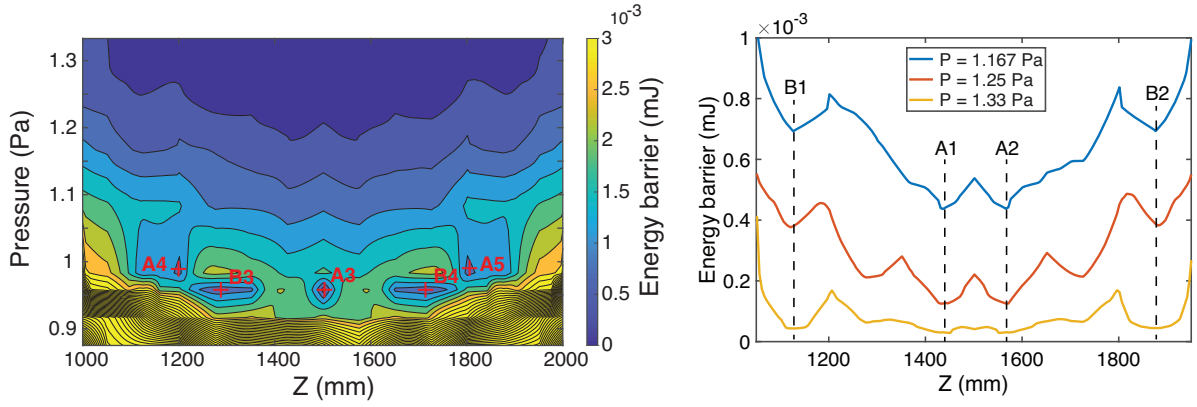

Fig. 16 (a) Contours of energy barrier for varying location of probe and pressure. (b) Detail of 3 high pressure energy barriers.

The situation changes if lower values of the pressure are considered in figure 16a. For $P = 0.96$ Pa, there is a global minimum for the energy barrier, A3, at the center of the strip ($Z = 1,500$ mm) surrounded by two local minima, B3, B4,

at $Z = 1,282$ mm and $Z = 1,722$ mm. The global minimum changes location rapidly and for $P = 0.98$ Pa the global minima are A4, A5 at locations $Z = 1,202$ mm and $Z = 1,802$ mm. These points are marked with a + in the figure. Note that the pressure at which these local minima occur is above the minimum post-buckling pressure for the strip structure.

The present analysis has shown that buckled equilibrium solutions exist for probing at these alternative locations, which cannot be determined by solving the classical buckling eigenvalue problem. An important observation is that the location of the lowest mountain pass points for the strip structure depends on the value of the pressure. In practice, the presence of these broken away modes can have a significant impact on the structure's post-buckling behavior. They can appear if the structure is subjected to realistic low intensity disturbances, such as vibration, and they can yield less advantageous post-buckling responses, such as a decreased post-buckling stiffness compared to the eigenmodes' post-buckling paths, and/or a lower value of maximum pressure. The implications of the existence of these modes on the structure's post-buckling regime will be discussed in a follow-on paper. Finally, although only antisymmetric probing was considered in the present study, similar results can be expected if only one longeron is probed locally. A single probe would allow the detection of more broken away modes; this is also a topic for a follow-on paper.

VIII. Effect of initial imperfections on strip stability landscape

It is well-known that thin shells are highly sensitive to geometric imperfections, and a natural question regards the sensitivity of the stability landscape to imperfections in the undeformed geometry. A preliminary investigation was carried out for the case $L = 1.8$ m, with imperfections based on the first eigenmode for longerons 1 and 2, as shown in figure 5a.

The imperfect structure was probed using the outward antisymmetric probing scheme at the location of the peak buckling mode displacement. In this specific case, the probing location also corresponds to the location of the maximum imperfection amplitude. The stability landscapes obtained for this specific probing scheme and for imperfection amplitudes ranging from 0% t to 50% t are shown in figure 17a. This figure shows that the imperfection has a significant impact on the structure's buckling load, which corresponds to the pressure above which the stability landscape can no longer be computed (the solver encounters the first bifurcation). For the perfect geometry, the buckling pressure is $P_{cr} = 3.3$ Pa which decreases to 2.9 Pa (88% of P_{cr}) for an imperfection amplitude of 10% t, 2.48 Pa (75% of P_{cr}) for an imperfection amplitude of 30% t, and finally reaches 2.08 Pa (63% of P_{cr}) for an imperfection amplitude of 50% t.

An important observation is that the minimum post-buckling pressure is barely affected by the imperfection for amplitudes under 40% t. For the perfect geometry, the minimum post-buckling pressure is $P_M = 2.26$ Pa. This value does not change for an imperfection of 10% t and decreases only slightly, to 2.22 Pa and 2.2 Pa for imperfection amplitudes of 30% t and 40% t, respectively. For a critical value of imperfection amplitude, between 40% t and 50% t, the buckling load equals the minimum post-buckling pressure and past this value of imperfection, the structure is no longer meta-stable. A final observation is that the energy barrier required to reach early buckling for the imperfect

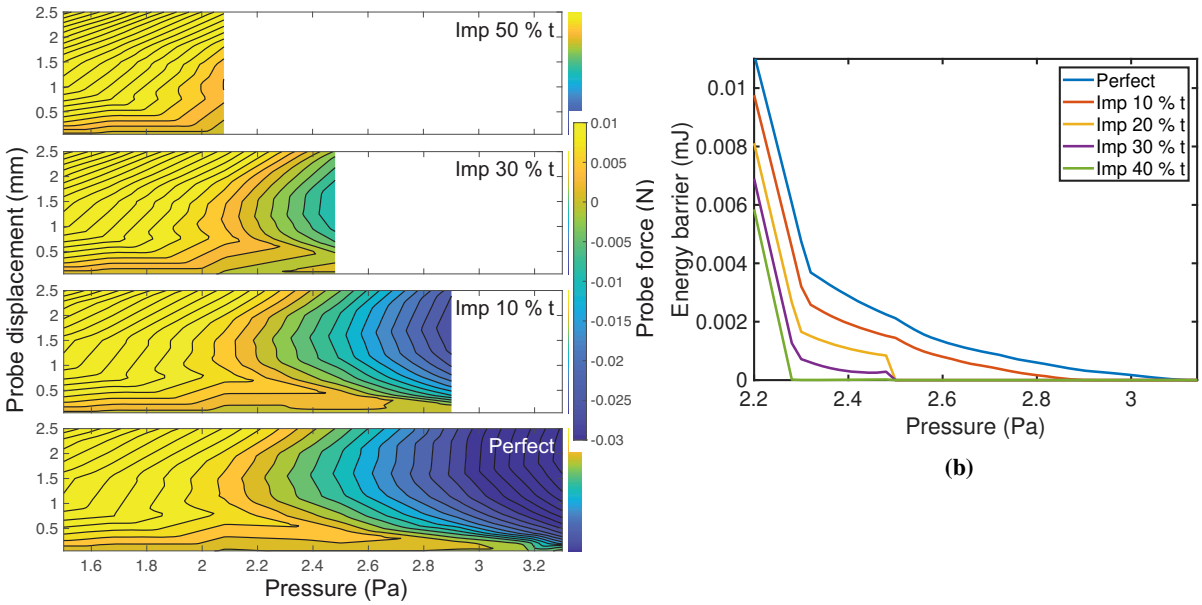

(a) **(b)**

Fig. 17 (a) 1.8 m strip stability landscape for antisymmetric probing with growing geometrical imperfections. (b) First buckling energy barrier with growing geometrical imperfections.

structure, shown in figure 17b, decreases when the imperfection amplitude increases, and there is a sudden drop for imperfection amplitudes above 10% t.

As a summary, this preliminary analysis has highlighted that, for imperfections based on the first eigenmode, there exists an amplitude threshold (between 40% t and 50% t) which separates two different buckling regimes: unstable and stable buckling. It is likely that larger imperfection amplitudes will be of practical interest, in which case the structure will no longer exhibit unstable buckling. However, in the present analysis, the eigenmode imperfection was chosen to coincide with the probing location, which is the worst case assumption. If the imperfection is located farther away from the probe, its impact on probing would be less significant and therefore larger amplitude are likely to exhibit an unstable buckling behavior.

Finally, whereas this study has considered only buckling mode imperfections, other types of imperfection such as global twist, have been observed in practice. It is generally found that eigenmode-based imperfections have the most detrimental effect on a structure's buckling behavior, and hence it is expected that other types of imperfection would have less impact on the probing sequence and the energy barrier erosion close to buckling. However, further work will be needed to more fully understand the interaction between probing and imperfections. Experiments will play an important role in this future research.

IX. Conclusion

This paper has presented a numerical study of the buckling and post-buckling behavior of structures of interest for large coilable solar arrays. The specific structure that has been studied is a ladder-type strip structure consisting of two coilable thin shell longerons connected by transverse battens. Its transition into buckled configurations has been captured by plotting its stability landscape. This landscape is a three-dimensional plot of three independent quantities, the force and displacement of a localized lateral disturbance, introduced on the strip using a probe, and the main loading parameter. In the present case, the stability landscape of a strip structure is a plot of probe force vs. probe displacement and vs. transverse pressure.

It has been shown that the stability landscape for a pressure-loaded strip is similar to the landscape for classical shells, such as the axially-loaded cylinder and the pressure-loaded sphere. Similarly to classical shells, the stability landscape for the strip shows that an early transition of the strip into buckling can be triggered by small disturbances, whose amplitude decreases when the main loading is increased. The most important difference between the behavior of the strip structure and the classical thin shells is that while the classical shell structures buckle catastrophically, the strip structure features a large stable post-buckling range. Therefore, the maximum post-buckling load that can be sustained by strip structures is significantly higher than the first buckling load.

The same probing technique used to derive the stability landscape for the strip to form its first buckle has also provided an effective way to investigate its post-buckling response and to gain insight into the meta-stability of the post-buckling path. This approach is especially useful when multiple successive buckles are encountered as the level of disturbance needed to form a specific series of buckles can be determined.

The probing of the structure's longerons was applied at multiple locations, and this analysis showed the existence of broken away paths (mountain pass points) corresponding to the single dimple in the cylinder and the sphere. The mode shapes for these specific early buckling paths localize at different locations than the ones predicted by a classical eigenvalue problem. An important take away for this problem is that the location of the lowest mountain pass point (minimum energy barrier to transition into buckling) is a function of the pressure applied to the strip.

The effect of imperfections, based on the first buckling mode, on the strip stability landscape has been assessed. While imperfections significantly degrade the buckling load and also erode the energy barrier separating pre-buckled from post-bucked states, it has been found that they have little impact on the minimum post-buckling pressure. It was also found that for a sufficiently large imperfection amplitude, the buckling load becomes as low as the minimum post-buckling pressure and the structure loses its meta-stability.

Regarding the practical design of strip structures, the present extension of the probing approach to more complex thin shell structures enables different design strategies. For applications in which buckling is to be altogether avoided, the structure can be designed such that it never exceeds the minimum post-buckling pressure. If upper bounds on the disturbance amplitude during operation and manufacturing deviations are known, the structure could be operated above

its minimum post-buckling pressure by using the energy barrier of the worst imperfect structure as the main design limit. Finally, in the case of a stable post-buckling regime and if small buckles during operation are acceptable, the ultimate failure load can be derived efficiently, numerically or experimentally, using the probing technique and can be used as a design criterion.

Lastly, for the specific strip structures that are of current interest [19] it has been shown that 0.2 m wide strips with lengths ranging from 1.5 m to 4.2 m have critical pressures from 5 Pa to 1 Pa, respectively. Under these loads, the structures will elastically collapse by folding around the center. The corresponding minimum post-buckling pressures range from 2.5 Pa to 0.5 Pa. For spacecraft applications it should be noted that these values are several orders of magnitude larger than solar pressure loading. For longer strips, knowledge of the strip stability landscape will be a crucial tool and the methods presented in this paper will play a key role in enabling the design of such structures.

Acknowledgments

The authors warmly thank John W. Hutchinson for help in preparing this paper. Financial support from the Space Solar Power Project at Caltech is gratefully acknowledged.

References

[1] von Kármán, T. and Tsien, H. S. (1941). The buckling of thin cylindrical shells under axial compression. Journal of the Aeronautical Science, Vol. 8, pp. 303-312. https://doi.org/10.2514/8.10722

[2] Donnell, L. H. and Wan, C. C. (1950). Effect of imperfections on buckling of thin cylinders and columns under axial compression. Journal of Applied Mechanics, Vol. 17, No. 1, pp. 73-83. https://doi.org/10.1115/1.4010060

[3] Koiter, W. T. (1945). On the Stability of Elastic Equilibrium (in Dutch with English summary). Thesis, Delft, H. J. Paris, Amsterdam, Holland.

[4] Weingarten, V. I. and Seide, P. and Peterson, J. P. (1968). Buckling of thin-walled circular cylinders. NASA Space Vehicle Design Criteria, NASA SP-8007.

[5] Hilburger, M. W. (2012). Developing the next generation shell buckling design factors and technologies. 53rd AIAA/ASME/ASCE/AHS/ASC Structures, Structural Dynamics and Materials Conference, AIAA-2012-1686. https://doi.org/10.2514/6.2012-1686

[6] Lee, A., López Jiménez, F., Marthelot, J., Hutchinson, J. W., Reis, P. M. (2016). The geometric role of precisely engineered imperfections on the critical buckling load of spherical elastic shells. J. Appl. Mech. 83, 111005. https://doi.org/10.1115/1.4034431

[7] Rahman, T., Jansen EL. (2010). Finite element based coupled mode initial post-buckling analysis of a composite cylindrical shell. Thin-Walled Struct. 48, 25–32. https://doi.org/10.1016/j.tws.2009.08.003

[8] Riks, E., (1979). An incremental approach to the solution of snapping and buckling problems. International Journal of Solids and Structures 15 (7), 529 –874551. https://doi.org/10.1016/0020-7683(79)90081-7

[9] Potier-Ferry, M. (1983). Amplitude modulation, phase modulation and localization of buckle patterns. In COLLAPSE: the buckling of structures in theory and practise (eds J.M.T. Thompson, G.W. Hunt). Cambridge, UK: Cambridge University Press.

[10] Horák, J., Lord, G.J., Peletier, M.A. (2006). Cylinder buckling: the mountain pass as an organizing center. SIAM J. Appl. Math. 66, 1793–1824. https://doi.org/10.1137/050635778

[11] Hunt, G.W., Lucena-Neto, E. (1993). Maxwell critical loads for axially loaded cylindrical shells. Trans. ASME 60, 702–706. https://doi.org/10.1115/1.2900861

[12] Thompson, J.M.T., van der Heijden, G. H. M. (2013). Quantified 'Shock-sensitivity' above the Maxwell load. International Journal of Bifurcation and Chaos 24.03 (2014): 1430009. https://doi.org/10.1142/S0218127414300092

[13] Virot, E., Kreilos, T., Schneider, T.M. and Rubinstein, S.M., (2017). Stability landscape of shell buckling. Phys. Rev. Lett. 119, 224101. https://doi.org/10.1103/PhysRevLett.119.224101

[14] Groh, R.M.J. , Pirrera A. (2019). On the role of localizations in buckling of axially compressed cylinders. Proc. R. Soc. A 475:20190006. http://dx.doi.org/10.1098/rspa.2019.0006

[15] Gerasimidis, S., Virot, E., Hutchinson, J. W. and Rubinstein, S.M. (2018). On establishing buckling knockdowns for imperfection-sensitive shell structures. J. Appl. Mech. 85-091010-1-14. https://doi.org/10.1115/1.4040455

[16] Arya, M., Lee, N. and Pellegrino, S. (2016). Ultralight structures for space solar power satellites. SciTech 2016, San Diego, AIAA-2016-1950. https://doi.org/10.2514/6.2016-1950

[17] Royer, F. and Pellegrino, S. (2018). Ultralight ladder-type coilable space structures. SciTech 2018. Orlando (FL), AIAA-2018-1200. https://doi.org/10.2514/6.2018-1200

[18] Gdoutos, E., Leclerc, C., Royer, F., Turk, D.A., and Pellegrino, S. (2019). Ultralight spacecraft structure prototype. SciTech 2019, San Diego (CA), AIAA-2019-1749. https://doi.org/10.2514/6.2019-1749

[19] Gdoutos, E. E., Truong, A., Pedivellano, A., Royer, and Pellegrino, S. (2020). Ultralight deployable space structure prototype. SciTech 2020, Orlando (FL), AIAA-2020-0692. https://doi.org/10.2514/6.2020-0692

[20] Murphey, T.W. and Banik, J., (2011). Triangular rollable and collapsible boom. U.S. Patent 7,895,795.

[21] Leclerc, C., Wilson, L., Bessa, M., and Pellegrino, S. (2017). Characterization of ultra-thin composite triangular rollable and collapsible booms. SciTech 2017, Grapevine (TX), AIAA-2017-0172. https://doi.org/10.2514/6.2017-0172

[22] Leclerc, C. and Pellegrino, S. (2020). Nonlinear elastic buckling of ultra-thin coilable booms. International Journal for Solids and Structures 203: 46-56. https://doi.org/10.1016/j.ijsolstr.2020.06.042

[23] Banik, J. A., and Murphey, T. W. (2010). Performance validation of the triangular rollable and collapsible mast. 24th Annual AIAA/USU Conference on Small Satellites, Logan, UT: AIAA/ASU.

[24] Murphey, T. W., Turse, D., and Adams, L. (2017). TRAC boom structural mechanics. 4th AIAA Spacecraft Structures Conference, AIAA-2017-0171. https://doi.org/10.2514/6.2017-0171

[25] Bessa, M. and Pellegrino, S. (2018). Design of ultra-thin shell structures in the stochastic post-buckling range using Bayesian machine learning and optimization. International Journal of Solids and Structures. 139-140, 174–188. https://doi.org/10.1016/j.ijsolstr.2018.01.035

[26] Healey, T. J. (1989). Why bifurcation: a study of a reticulated dome. American Society of Civil Engineers, Structures Congress '89, Sessions related to design, analysis and testing. San Francisco, California.

[27] Peterson, M. E. and Murphey, T. W. (2013). Large deformation bending of thin composite tape spring laminates. In 54th AIAA/ASME/ASCE/AHS/ASC Structures, Structural Dynamics, and Materials Conference, AIAA-2013-1667. https://doi.org/10.2514/6.2013-1667

[28] Thompson, J.M.T., Hutchinson, J.W., Sieber, J. (2017). Probing shells against buckling: a nondestructive technique for laboratory testing. International Journal of Bifurcation and Chaos. 27. https://doi.org/10.1142/S0218127417300488

[29] Groh, R.M.J., Avitabile, D., Pirrera, A. (2018). Generalised path-following for well-behaved nonlinear structures. Comput. Methods Appl. Mech. Eng. 331, 394–426. https://doi.org/10.1016/j.cma.2017.12.001

[30] Pirrera, A., Avitabile, D., Weaver, P.M. (2010). Bistable plates for morphing structures: A refined analytical approach with high-order polynomials. International Journal of Solids and Structures, volume 47, issues 25–26. https://doi.org/10.1016/j.ijsolstr.2010.08.019

[31] Wadee, M.K. , Hunt, G.W. , Whiting, A.I.M. (1997). Asymptotic and Rayleigh-Ritz routes to localized buckling solutions in an elastic instability problem. Proc. R. Soc. A 453, 2085–2107. https://doi.org/10.1098/rspa.1997.0112

[32] Audoly, B., and Hutchinson, J.W. (2019). Localization in spherical shell buckling. Journal of the Mechanics and Physics of Solids, https://doi.org/10.1016/j.jmps.2019.103720

[33] Thompson, J.M.T., Sieber, J. (2015). Shock-sensitivity in shell-like structures: with simulations of spherical shell buckling. Int. J. Bifurcation Chaos 26, 1630003. https://doi.org/10.1142/S0218127416300032

[34] Hutchinson, J.W. (2016). Buckling of spherical shells revisited. Proc. R. Soc. A 472, 20160577. https://doi.org/10.1098/rspa.2016.0577

[35] Hutchinson, J.W., Thompson, J.M.T. (2017). Nonlinear buckling behaviour of spherical shells: barriers and symmetry-breaking dimples. Phil. Trans. R. Soc. A 375, 20160154. https://doi.org/10.1098/rsta.2016.0154

[36] Hunt, G.W., Peletier, M.A., Champneys, A.R., Woods, P.D., Wadee, M.A., Budd, C.J., Lord, G.J. (2000). Cellular buckling in long structures. Nonlinear Dynamics. 21, 3–29. https://doi.org/10.1023/A:1008398006403